ISSN 1063-7729, Astronomy Reports, 2019, Vol. 63, No. 8, pp. 652–665. © Pleiades Publishing, Ltd., 2019.
Russian Text © The Author(s), 2019, published in Astronomicheskii Zhurnal, 2019, Vol. 96, No. 8, pp. 638–652.

An Unusually Powerful Water-Maser Flare in the Galactic Source W49N

L. N. Volvach[1*], A. E. Volvach[1,2], M. G. Larionov[3], P. Wolak[4], B. Kramer[5], K. Menten[5], A. Kraus[5], J. Brand[6,7], A. Zanichelli[6], S. Poppi[8], S. Rigini[6], A. V. Ipatov[2], D. V. Ivanov[2], A. G. Mikhailov[2], and A. Mel'nikov[2]

[1]*Department of Radio Astronomy and Geodynamics, Crimean Astrophysical Observatory, Katsivelli, Russia*
[2]*Institute of Applied Astronomy, Russian Academy of Sciences, St. Petersburg, 191187 Russia*
[3]*Astro Space Center, P.N. Lebedev Physical Institute, Russian Academy of Sciences, Moscow, 117997 Russia*
[4]*Torun Centre for Astronomy, Nicolaus Copernicus University, Piwnice, PL-87-148 Lysomice, Poland*
[5]*Max-Planck-Institut für Radioastronomie, Auf dem Hügel 69, D-53121 Bonn (Endenich), Germany*
[6]*INAF—Istituto di Radioastronomia, 40129 Bologna, Italy*
[7]*Italian ALMA Regional Centre, Bologna, Italy*
[8]*INAF—Osservatorio Astronomico di Cagliari, 09047 Selargius (CA), Italy*

Received November 14, 2018; revised March 15, 2019; accepted March 22, 2019

Abstract—The most powerful flare ever registered in the Galactic water-maser source W49N has been detected in long-term monitoring data in the 6_{16}–5_{23} transition with line frequency $f = 22.235$ GHz carried out on the 22-m Simeiz, 32-m Toruń, 100-m Effelsberg, and 32-m Medicina radio telescopes, beginning in September 2017 and continuing in 2018. Some stages of the flare were monitored daily. Detailed variations of the source spectral flux density with time have been obtained. At the flare maximum, the flux exceeded $P \approx 8 \times 10^4$ Jy, and this was record highest flux registered over the entire history of observations of this source. Important conclusions related to details of the mechanism for the H_2O line emission have been drawn. An exponential increase in the flare flux density was detected during both the rise and decline of the flare. The data obtained indicate that the maser is unsaturated, and remained in this state up to the maximum observed flux densities. Additional support for the idea that the maser is unsaturated is the shape of the dependence of the line width on the flux. The characteristics of the variations of the spectral flux density are probably associated with a sharp increase in the density of the medium and the photon flux that led to an increase in the temperature from an initial level of 10–40 K to hundreds of Kelvins. Interferometric maps of the object during the increase in the spectral flux density of the flare have been obtained. A possible mechanism for the primary energy release in W49N is considered.

DOI: 10.1134/S1063772919080067

1. INTRODUCTION

The maser transition (6_{16}–5_{23}) water-maser transition was first discovered in cosmic sources in 1969, as part of the 2μ sky survey [1, 2]. A large number of water masers were found in these survey data, among them W49N, which is one of the brightest known sources of maser emission [1, 2].

The maser source W49N is associated with an HII region with compact radio emission having a radius of less than 3.5″ [3, 4]. This angular size corresponds to ~0.32 pc for a distance to the object of 11 kpc [5].

Multiple water-maser lines are registered in the object over a wide range of velocities, ±300 km/s. Most of these are concentrated in a compact region (0.1 pc). It was noted that sources located in such a small volume and having such a large velocity dispersion cannot form a dynamically stable system [6].

Another problem is explaining the broad range of velocities of the water-maser emission lines in W49N (≈600 km/s). This cannot be explained by accretion of the matter onto a protostar, since the accretion flow velocities are no more than a few tens of km/s [7]. With this in mind, other acceleration mechanisms have been suggested: stellar winds from hot massive stars, radiative pressure, shocks [6], and even a rarer phenomenon associated with supernova explosions [8]. However, a detailed physical picture of these processes remains incompletely understood.

Low-velocity features of the water-maser line display significant flux-density variability ranging from

*E-mail: volvach@bk.ru

hours to many years. Detailed monitoring of the flux density has detected an increase to 80 kJy [9].

Early interferometric data indicated a multi-component structure of the region of H_2O emission. According to [10, 11], there are six main regions of water line emission within a $3'' \times 1.5''$ area. There have also been attempts to detect linear polarization [12].

The time delays between the emission components in W49N in its maser region with a size of $\sim 2 \times 10^{17}$ cm corresponds to the propagation of a perturbation at the speed of light. This may point toward radiation pumping of the maser [13].

The complex structure of the components of the water-maser lines in W49N and significant blending of these components were noted. This substantially hinders interperation of the observational data and the construction of a physical picture of the water-maser emission in this object.

The general picture of the H_2O emission region is the following. In a dense medium of molecular hydrogen, in envelopes around protostars, heating of the medium takes place, by factors including adiation, shocks, protostellar ejections, and the accretion of matter. The abundance of H_2O relative to hydrogen can be appreciable, $\sim 10^{-4}$—four to five orders of magnitude higher than the average relative water abundance in the Galaxy [14–16]. Water molecules that evaporate at temperatures close to 130 K become predominant in the gaseous component of protostars, along with CO molecules. This can explain the high fluxes in water-maser flares arising in star-forming regions in HII zones.

Water masers are also associated with other maser lines, in particular OH lines. This was pointed out by Gwinn et al. [17], who noted that the shock dissociation of H_2O in the presence of hydrogen and an influx of energy leads to the appearance of Type I OH emission [17]. However, there is no solid evidence for a close relationship between the emission in these lines.

In our current study, we present the results of long-term monitoring of W49N in the 22-GHz H_2O maser line. A powerful flare was detected, which is one of the strongest over the entire time this object has been observed. A possible interpretation of the experimental data is proposed.

2. OBSERVATIONS AND REDUCTION

The spectral–polarimetric radiometer and parallel-type spectral analyzer used to receive and record the water-line signals from the sources observed on the 22-m Simeiz radio telescope had 512 and/or 2048 channels and a radial-velocity resolution of 8 and 2 kHz (105 and 26 m/s), respectively [18]. The spectral data were corrected for atmospheric absorption (τ) and variations of the effective area of the radio telescope (A_{eff}) as a function of the antenna elevation. The receiver bandwidth was 4 MHz when the Mark 5B+ recording system was used and 16 MHz when the RDR1 recorder was used. The system noise temperature T_{sys} and absorption in the atmosphere were determined using a calibration step (noise generator), reduced to the aperture of the radio telescope using a matched load located in the feed horn at room temperature and at liquid-nitrogen temperature, and atmospheric cuts. This procedure is necessary to account for attenuation and noise signals inserted between the input of the feed horn and front amplifier. The temperature T_{sys} varied within 150–200 K, depending on the weather conditions. The flux calibration was performed using the sources DR 21, Vir-A, and Cyg-A. The radio telescope beam width at 22 GHz was 150″, and the corresponding sensitivity was 13 Jy/K.

Circular and linear polarization were used when the data was received in modes separated in time. When circular polarization was received, we used a polarizer whose operation is based on the Faraday effect. The digital output signal of the radiometer was integrated over three minutes for each rotation of the polarization plane of the polarizer by a fixed angle, and was recorded by the spectral analyzer. The antenna temperature T_{ant} of the received signal was calibrated using the signal from the noise generator.

A high-sensitivity 1.35 cm receiver system was installed at the secondary focus of the Simeiz 22-m telescope. The tunable heterodynes were synchronized using a highly stable 5 MHz signal from a VCH-1005 hydrogen-maser frequency standard, and enabled conversion of the input frequencies to intermediate frequencies within the above waveband [19]. In a single cycle of observations of the water-maser lines, the signal was accumulated for 5–10 minutes pointing at the target, and then pointing one arcsecond away from the target. This cycle could be repeated to achieve the necessary signal-to-noise ratio.

The observations on the 100-meter Effelsberg radio telescope were conducted with a 1.3 cm receiver installed at the secondary focus. The center frequency was 22.235 GHz, and the width of the emission pattern was $\sim 38''$. Spectral observations were performed using an FFT spectrometer with 65 535 channels. The bandwidth was 100 MHz, and the velocity resolution was about 20 m/s. The spectral data were corrected for atmospheric absorption and the dependence of the telescope sensitivity on the elevation. The conversion from antenna temperature to flux density was determined using continuum

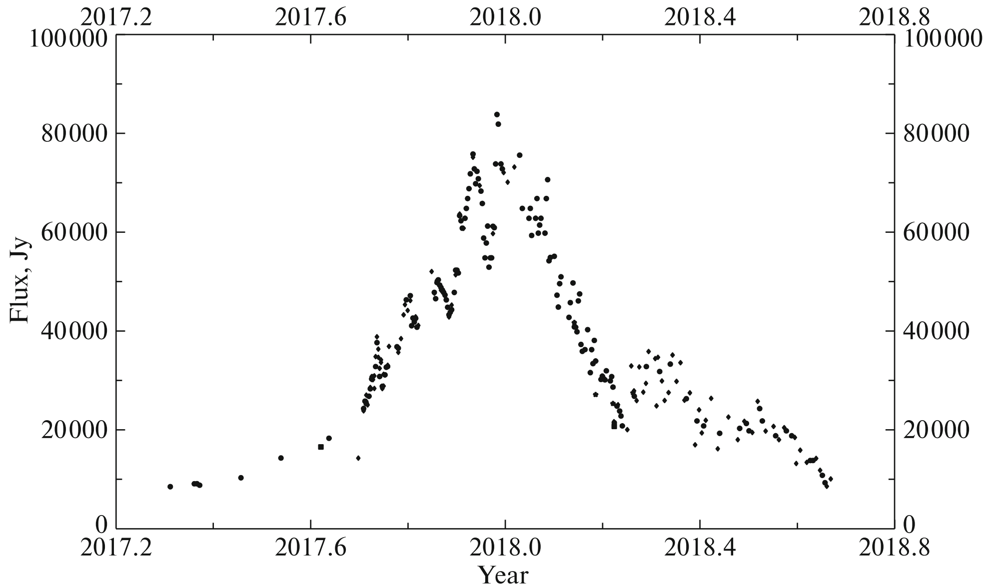

Fig. 1. Long-time monitoring of W49N in the water line (circles show the data obtained at Simeiz, diamonds the data from Toruń, squares the data from Effelsberg, and asterisks the data from Medicina).

observations (in cross-scan mode) of the calibration sources 3C286, NGC7027, and others [20].

The data acquisition for the 32-m Toruń and Medicina telescopes was similar to the data acquisition with Effelsberg. The digital autocorrelator employed at Toruń had 4096 channels and a velocity resolution of 26 m/s.

3. MONITORING OF THE SPECTRAL FLUX DENSITY OF W49N IN THE H_2O LINE

Regular long-term monitoring of W49N began in September 2017 and was performed in parallel with observations of the maser IRAS 18316-0602, in which a powerful flare was developing at that time. Spectral observations were made at intervals of one to two days. Figure 1 shows the dependence of the spectral flux density in the water line at a velocity close to 6 km/s, derived from the line maximum.

As in the case of flares of the maser sources in Orion KL, IRAS 18316-0602, such variations of the spectral flux density may indicate sharp changes in the physical characteristics in the regions of water-maser emission. These changes could be associated with a sharp injection of energy that led to an increase in the temperature and density of both the matter of the globule itself and of the incident radiation.

We attempted to obtain agreement between the data obtained at different telescopes to within 5–10 %. The source fluxes on specific observing dates were compared. It should also be noted that the daily amplitude variations near the maximum values can reach tens of percent if the growth is exponential (see, e.g., [30]).

According to [5], W49N is located 11 kpc from the Sun, and is one of the most distant masers in our Galaxy. The distance to the maser can be used to estimate the bolometric luminosity of the associated IR source and the spectral type of the exciting star. Taking into account the excitation parameter required for the compact HII region ($u = 110$ pc/cm^2) and the integrated infrared luminosity, The central source of primary energy release must be a massive, early-type O5 star with a luminosity of $L \sim 4 \times 10^6\ L_\odot$ [21]. This means that we are dealing with a hot giant with a mass of tens of solar masses that is able of ionizing the dense ambient environment out to a distance of 10^{17}–10^{18} cm.

Thus, W49N, together with IRAS 18316-0602, are the most powerful Galactic kilomasers. If W49N were at the distance of Orion KL, its flux would be 50 000 kJy, almost a factor of ten higher than the maximum of the most powerful flare in Orion over the entire time of its observations (≈6000 kJy).

The giant flare of the water maser in W49N began in April 2017 and continued in 2018. Our analysis of the flux density variations during the flare leads to important conclusions.

The shape of the flare is not symmetric. The slopes can be fitted by exponential functions. The exponential shape of the flux density variations is consistent with the maser being unsaturated during the flare, so that the amplification of the maser grows exponentially, also with an exponential growth of the optical depth [22].

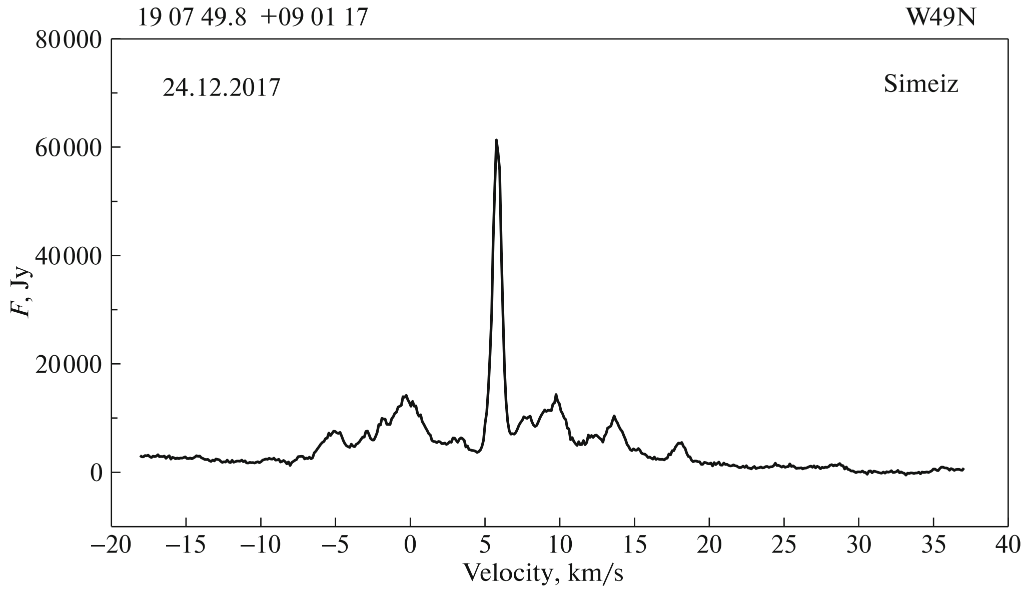

Fig. 2. The water line in W49N at the flare maximum.

The symmetric shape of the central part of the maser line in W49N close to the maximum phase and the decrease of the line half-width to 50 kHz argue in favor of an one-component source being responsible for the bulk of the increase in flux density. Examples of water line recordings near the flare maximum of 2017–2018 are shown in Figs. 2 and 3.

The line that is close to zero velocity (relative to the local system of rest) has a spectral flux density in excess of 15 kJy. Twelve lines resolved by the spectrometer have flux densities exceeding 5 kJy. If W49N were at the distance of Orion KL, these lines would have spectral flux densities exceeding 5000 kJy, almost equal to the most powerful flare in Orion KL, which occurred in 1998 [24].

In May 2017, the component with a velocity close to 6 km/s had a flux density below 10 kJy, while the flux from the nearest components was a factor of 1.5–2 higher (Fig. 4). In mid-August 2017, during the rise stage of the flare, there was a time when the line components closest to the center had similar spectral fluxes of about 16 kJy (Fig. 5). The amplitudes of these lines did not change up to the flare maximum (December 24, 2017, see Fig. 2).

There is strong blending on the slopes of the flare below 5000 Jy, due to many line components falling into the radio telescope beam. Examples of line recordings up to the level of 15 kJy are presented in Figs. 3b, 4, and 5. These examples show that this line is narrow. Analysis of the line shape leads to the conclusion that it reflects the emission of a single globule. Neighboring lines are significantly blended by the emission of several globules. Figure 2 shows an example of a line recording during the flare maximum on December 24, 2017.

At the beginning of 2018, the maser source remained close to the flare maximum and had a spectral flux density close to 75 kJy (Figs. 6a, 6b). Figure 7 shows the spectrum of low-velocity lines in W49N during the exponential decrease of the spectral flux density of the flare.

As in the case of the giant flare of IRAS 18316-0602 in 2017–2018, the line widths display a dependence on the flux in the flare we consider here. This dependence is shown in Fig. 8 in a plot of ΔV^{-2} versus $\ln F$, where F is the flux density at the line maximum in Jy and ΔV is the line width at the half-maximum level in km/s. The observational data are shown as points in this plot. They can be described well the straight line shown. At the activity maximum, the line is symmetric and can be described by a Gaussian.

This dependence of the line width on the flux may indicate that the maser is unsaturated. Similar results were obtained for giant flares in Orion KL and IRAS 18316-0602 [23, 24]. In both cases, it was concluded that the masers remained in an unsaturated state right up to the flare maximum.

Multiple stars at the center of the nebula could also provide the observed infrared luminosity, with the spectral type of the most massive star being O5. These stars are among the most massive in the Galaxy.

Bologna et al. [25] did not detect linear polarization in W49N at the 1% level. This enabled them to use this source to calibrate the instrumental polarization.

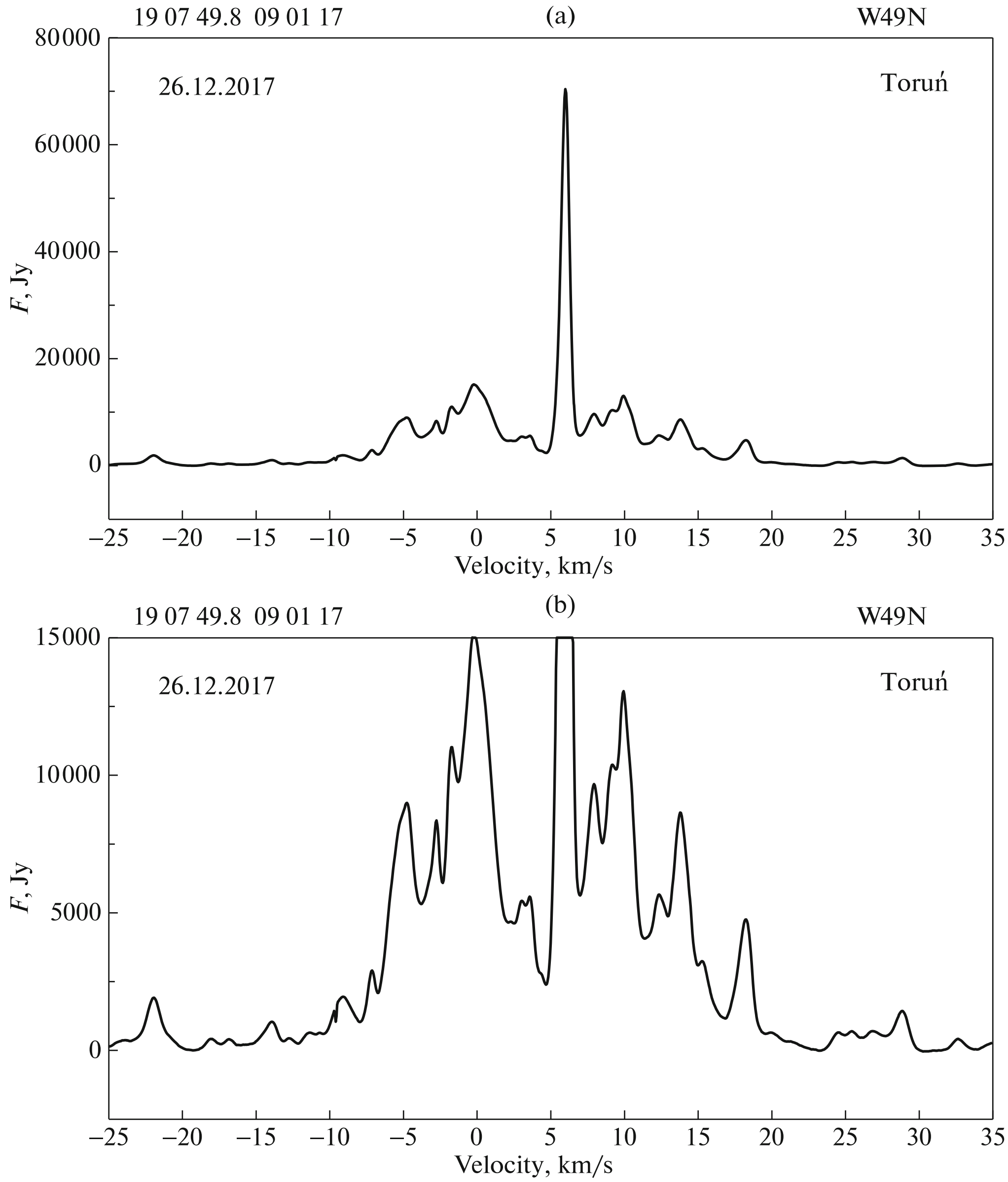

Fig. 3. (a) Example of a recording of the water line in W49N close to the flare maximum. (b) Example of a recording of the water line in W49N close to the flare maximum below a flux of 15 kJy.

4. INTERFEROMETRIC OBSERVATIONS

Interferometric data on the structure of the water masers in W49N indicate that the regions of emission are concentrated in individual active sites with dimensions $\sim 10^{16}$ cm. About a dozen of these occupy a total area $\sim 3 \times 10^{17}$ cm in size [10, 26, 27]. It is believed that the areas of activity are somehow related to young massive stars in the pre-main-sequence stage.

Unprecedented blending is observed in the object, both in spatial arrangement and in the spectrum. According to the above studies, more than half of all the maser sources in this region have components within 1.0 km/s of each other in the spectrum. Such values can also be reached by drifting of the line frequency with time, even in an isolated maser source. Therefore, if changes in the frequency of a component are observed over some time, it is unclear whether one this is due to a drift in the line frequency in a single source or the appearance of another source with similar frequency characteristics. This illustrates the complexity of interpreting the physical picture in such a complex radio source.

Nevertheless, the successes of interferometric observations cannot be underestimated. Already in 1973, limits on the sizes of bright maser globules in W49N were derived: $<5 \times 10^{-4}$ arcsec. Given the

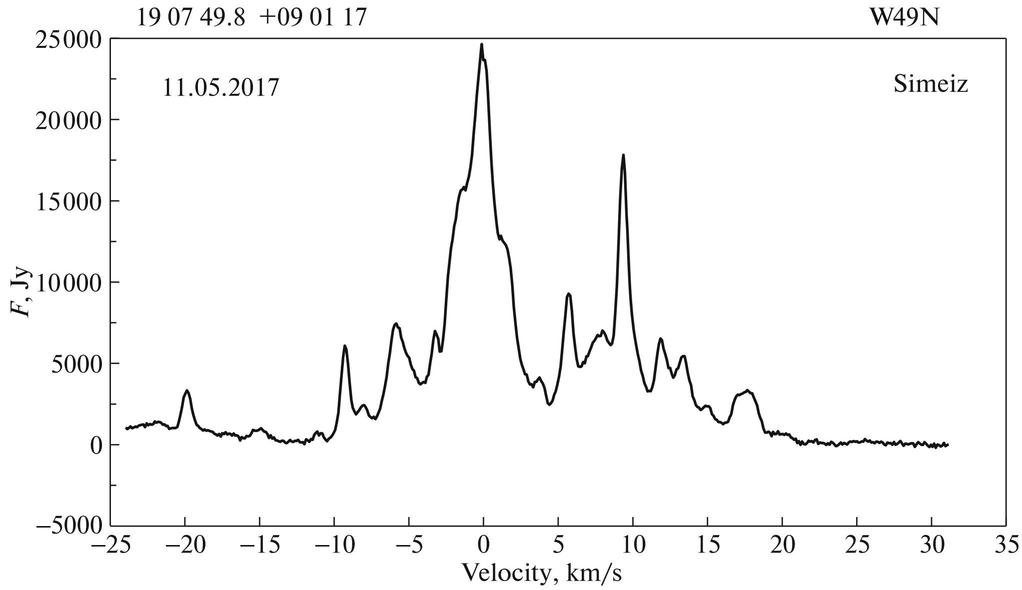

Fig. 4. Rise phase of the spectral flux density during the flare in W49N.

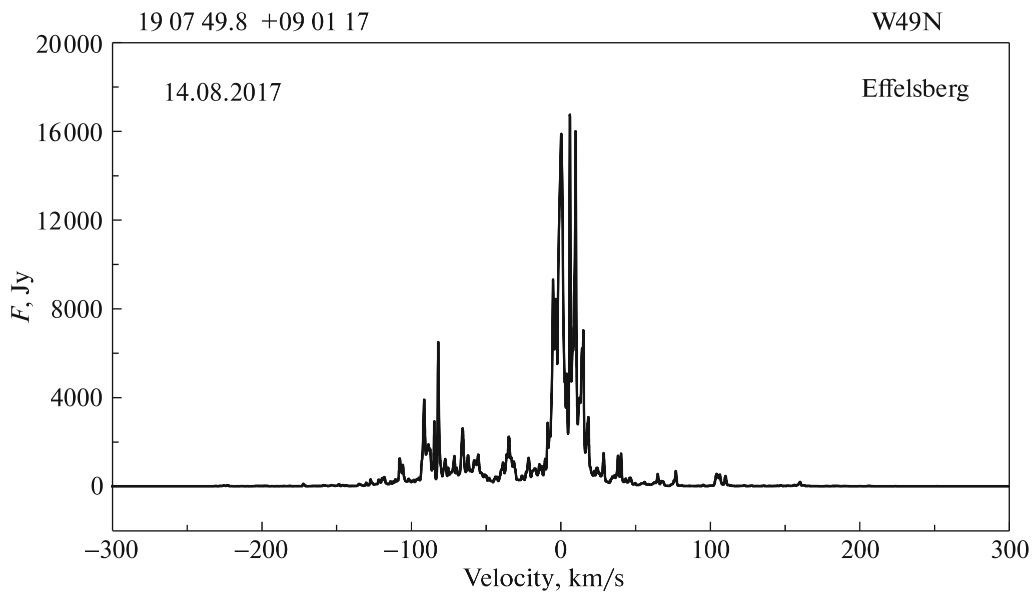

Fig. 5. Rise phase of the spectral flux density during the flare in W49N.

distance to the source, this corresponds to less than 5 AU [10].

The water-maser source in W49N was observed in interferometric mode in September 2017 on four days (September 17, 18, 26, and 27). The interferometer consisted of three 32-m radio telescopes of the Kvazar–KVO VLBI complex and the 22-m radio telescope of the Simeiz VLBI station. In the VLBI observations, the beginning of the band was set to 22.229 GHz, and each scan of the source was 20 min. The source 3C454.3 was selected as a calibrator, and 5-min or 20-min scans were observed at the beginning, middle, and end of the session. The correlation of the VLBI observation was carried out using the DiFX 2.4.1 software correlator of the Institute of Applied Astronomy, on a hybrid blade server cluster. The maps obtained for September 18 and 27, 2017, when the flux density of the source was rising, are shown in Figs. 9 and 10. Figures 11 and 12 show the spectra of low-velocity lines obtained during the interferometric sessions.

In the maps presented in Figs. 9 and 10, one arcsec corresponds to a linear scale of about 13 AU, based on a distance to W49N of 11 kpc. With such

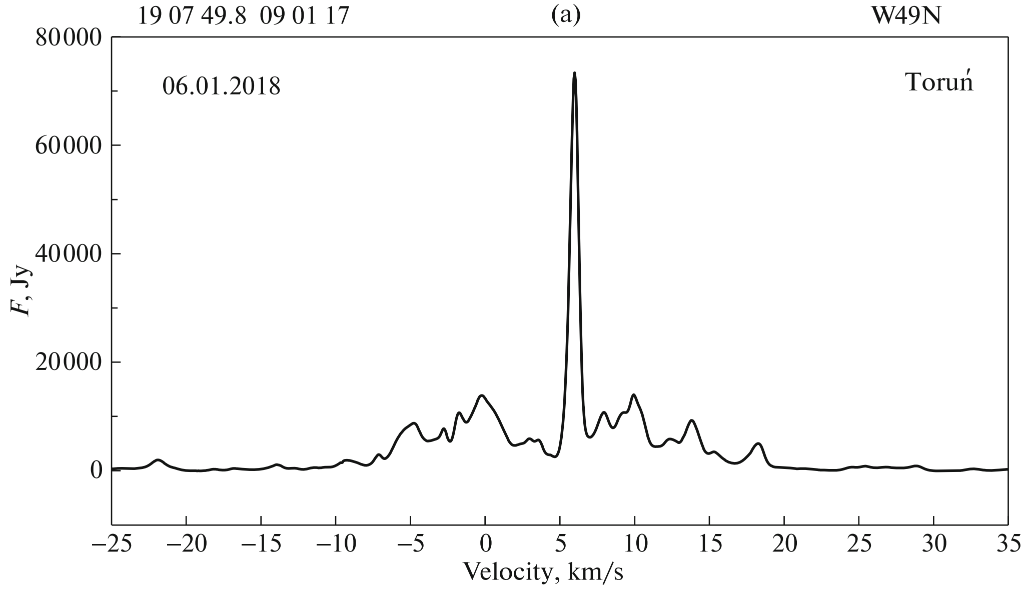

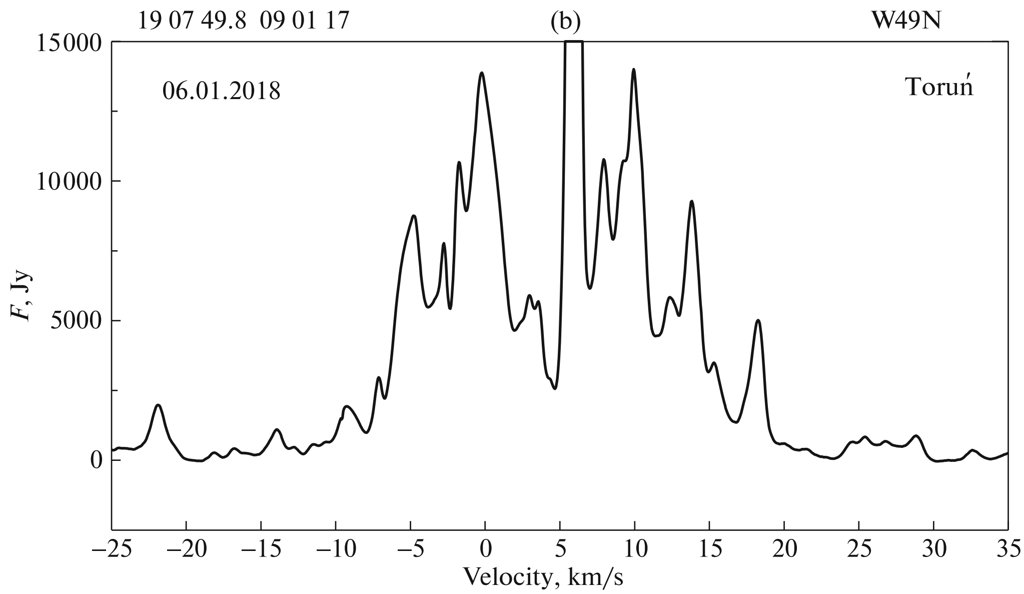

Fig. 6. (a) Maser line at the maximum before the onset of the decline of the spectral flux density. (b) Maser line at the maximum before the onset of the decline of the spectral flux density below a flux of 15 kJy.

resolution, the separate sources of maser emission remain unresolved. Given that ground VLBI observations can provide only a factor of two higher resolution, only ground–space experiments would be able to fully resolve the emission regions. However, the overall pattern of the brightness distribution in this object is observed fairly clearly. The bright central feature can be associated with the source of maser emission in which the powerful water-maser flare occurred. There are essentially no other features in the map.

Figure 13 shows the state of the lines on the descending branch of the maser flare in W49N. The structure of adjacent lines has changed significantly. Extreme blending along the line of sight and in frequency makes it difficult to determine the parameters of the individual maser sources, which stand out only during strong flares. During these periods, their spectral flux density is substantially higher than for the remaining sources, and it is possible to determine the coordinates, maser frequency, parameters, and temporal characteristics of the source. These data are consistent with observations of other powerful Galactic maser emission sources, which indicate that compact HII regions have dimensions $l_{\mathrm{HII}} \approx 10^{16}$ cm [27]. The molecular disks where the maser sources can reside have dimensions $l_{\mathrm{disk}} \geq 10^{17}$ cm (10^4 AU). The

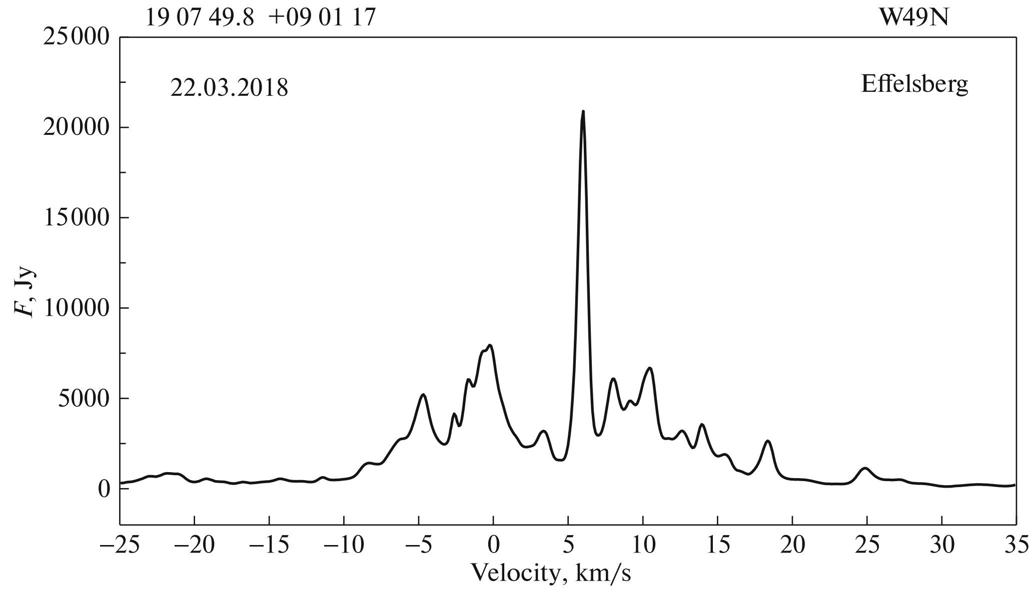

Fig. 7. Behavior of the flare line spectrum in the decline phase of the spectral flux density.

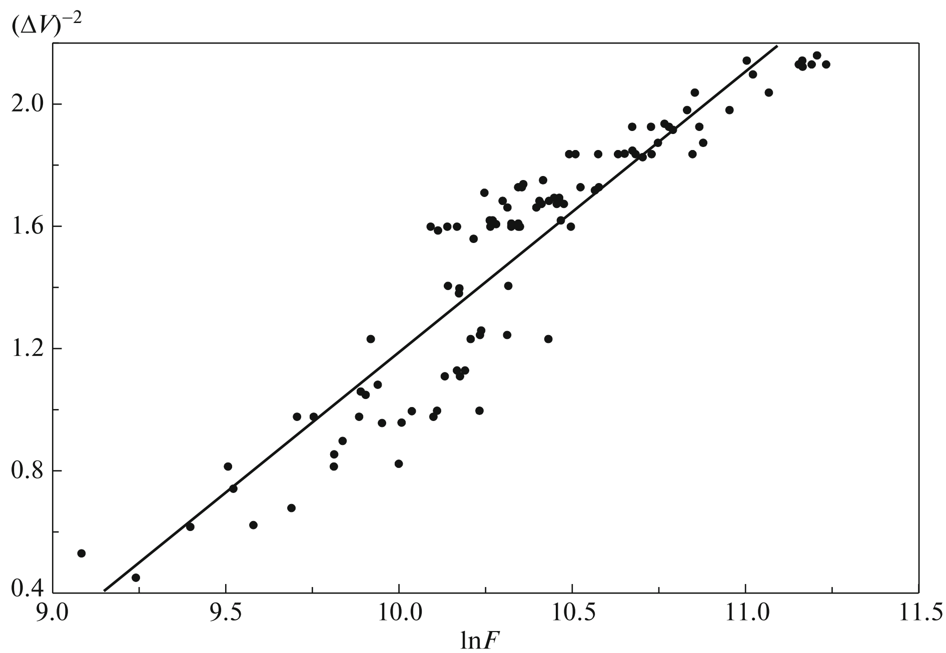

Fig. 8. Dependence of the line width of the water-maser line on the flux during the flare in W49N in 2017–2018.

maser sources themselves probably have sizes below 1 AU.

Thus, interferometric data obtained during the water-maser flare in W49N are consistent with other data suggesting the presence of individual compact formations responsible for substantially increasing the flux density in the object.

To conclude this section, we would like to note one more important circumstance regarding the dependence of the spectral flux density during the flare in W49N (Fig. 1). The flux variations are strikingly similar to the giant flare in Orion KL, having the same overall shape and duration [24]. It was also concluded in [24] that that maser was in an unsaturated state during the flare.

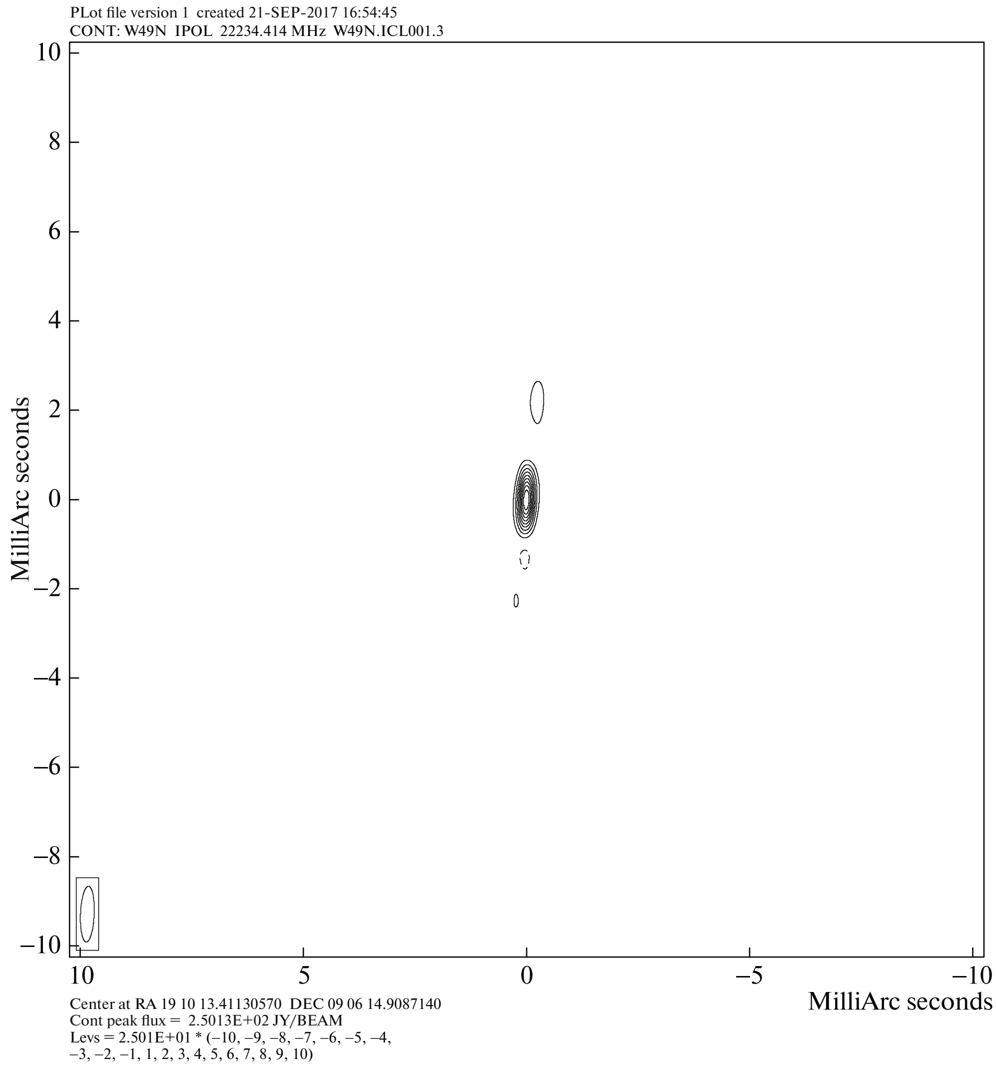

Fig. 9. Interferometric map of W49N obtained on KVAZAR–Simeiz baselines on September 18, 2017.

5. POSSIBLE SOURCES OF PRIMARY ENERGY RELEASE IN W49N

There are several opinions about the sources of primary energy release being discussed. The gigantic increase in the flux densities of water masers during flares must be a consequence of some powerful source of primary energy release.

The observed rapid changes in the spectral flux densities of lines must somehow be associated with changes of the activity of a central massive star. However, there remains the important question of what initiates changes in the behavior of the central object that can lead to such powerful flares in the water masers?

Any suggested model for the primary energy release in a system of maser sources must explain the complex of observed manifestations, including both low-velocity powerful flares of the maser emission and high-velocity maser features. The durations of the flares are more than a year (Fig. 1). The activity of the maser continues for six months, after which the flux density decreases. The possibility that there is one main maser condensation is indicated by the presence of a narrow emission line at a fixed frequency with a Gaussian profile. The observed parameters of the line seem to require a high density and considerable mass for the region of formation of the maser, together with a high temperature increase persisting over an appreciable period lasting several months. We must identify the physical process initiating the changes in the central object that lead to variations of these maser characteristics over the indicate time scale, with a very rapid rise and decline of the maser emission. All proposed water-maser pumping mechanisms encounter difficulties in explaining the giant energies of flares. Pumping by radiation from the central star and related phenomena cannot provide

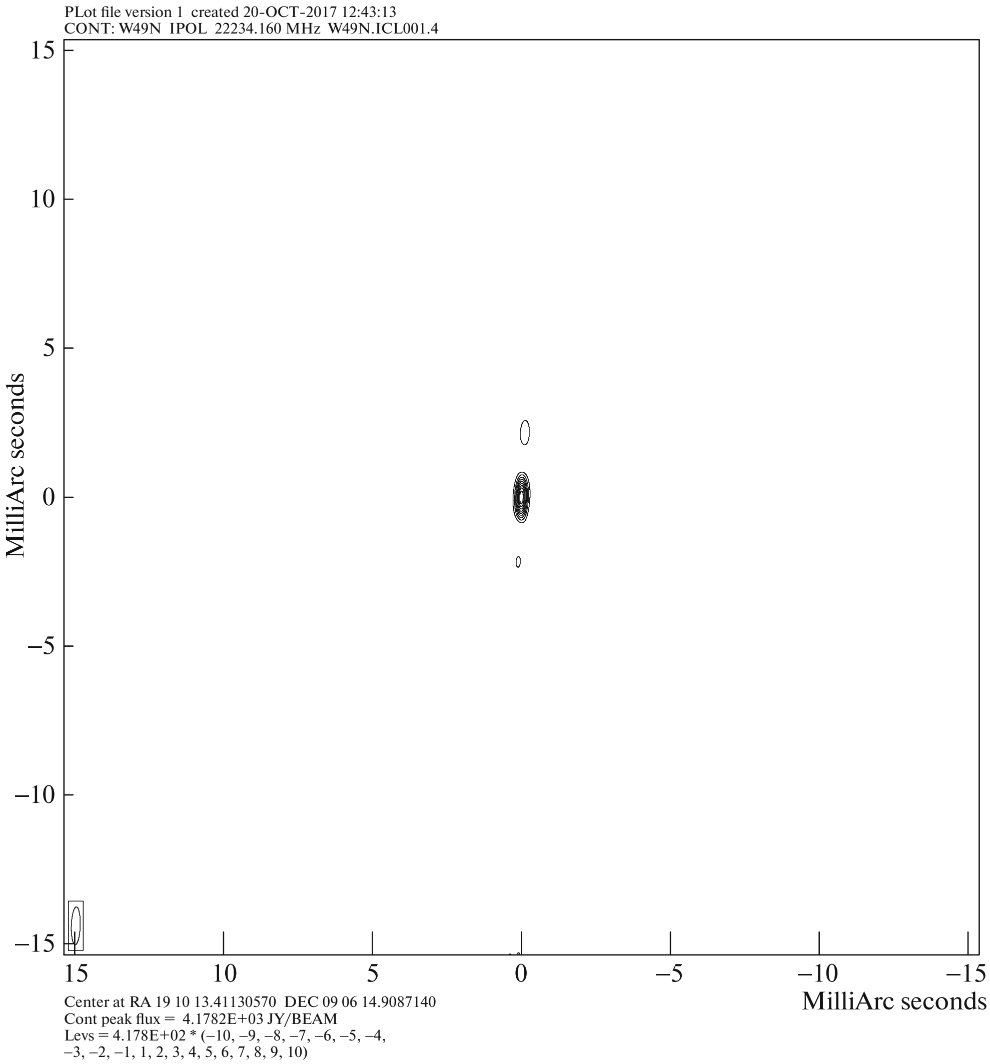

Fig. 10. Interferometric map of W49N obtained on KVAZAR–Simeiz baselines on September 27, 2017.

the line luminosities observed during super-powerful flares. The primary energy-release mechanism must be able to provide the necessary energy at the maxima of giant flares and explain why the central engine makes a transition to a state with the release of a huge amount of energy, exceeding the energy in the quiescent state by a factor of thousand or more.

One model that has been suggested involves pulsationally unstable massive stars [28]. In this case, it was attempted to explain the expected cyclic flares as an effect of colliding stellar winds in binaries [29]. The idea that the massive stars involved are binary seems to us to be useful. In [30], we developed these ideas for the case of multiple massive stars, when a quasi-periodic component of the water-maser emission is present in the object. The idea of initiating the primary energy release in massive, early-type multiple stars through the partial loss of the envelope of the central star under the influence of a fairly massive companion at the periastron of their orbit has been proposed.

It is natural to suppose that an appreciable fraction of massive stars in early evolutionary stages belong to double and multiple systems formed in the evolution of gas–dust clouds. When massive close binaries are formed, a powerful gravitational interaction arises between their components. This raises the possibility of inducint sources of primary energy release in gas–dust clouds through the partial loss of the envelope of the central massive star, due to the gravity of its companion at the orbit periastron. The episodic ejection of stellar envelopes could, in principle, provide the energy required for the considered process and explain giant maser flares that occur episodically every 10–20 years. Such ejections could be asymmetric, with the preferred direction of ejection depending on the orientation of the orbit. This could explain the observed predominance of high-speed lines of different

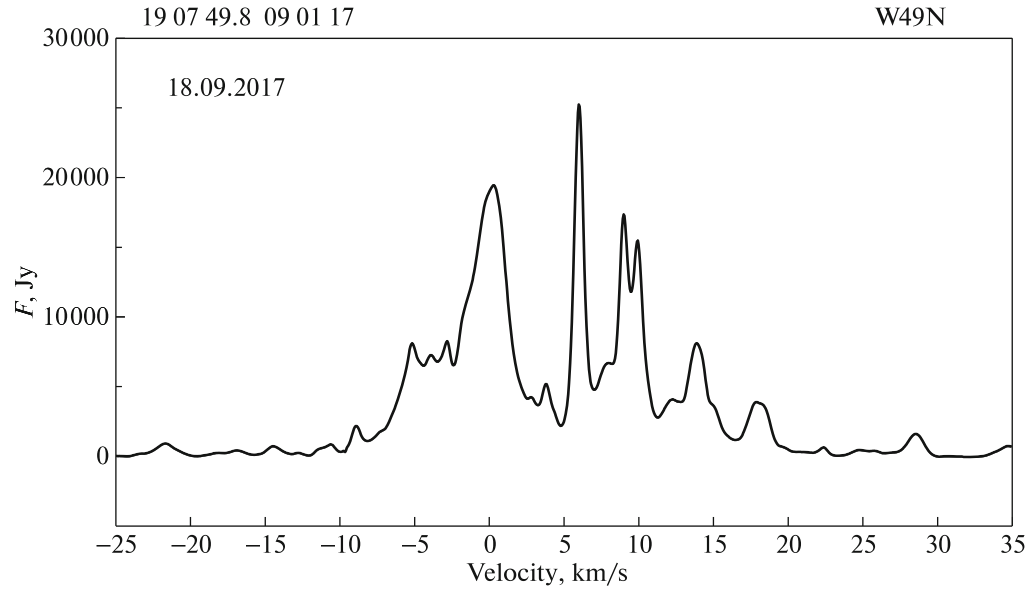

Fig. 11. State of low-velocity lines in the spectrum of W49N on September 18, 2017, when interferometric observations were performed.

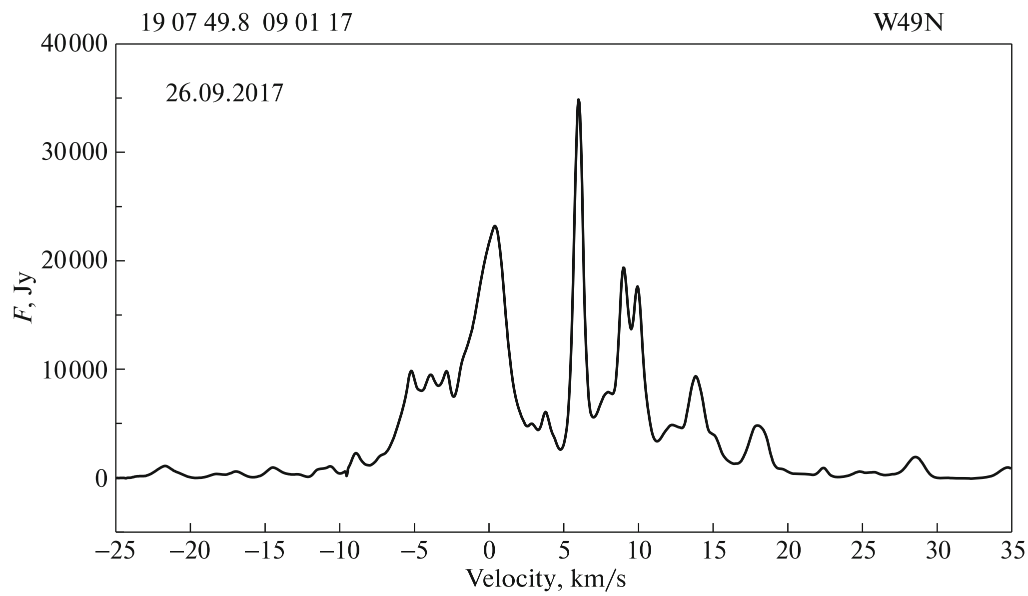

Fig. 12. State of low-velocity lines in the spectrum of W49N on September 26, 2017, when interferometric observations were performed.

signs in different systems. In addition, due to projection effects, both low-speed and high-speed lines are observed in the same object.

In the case of W49N, the superflare continued for more than a year. The presence of a high-velocity feature in the source (with a velocity close to 100 km/s) would imply a velocity for the ejected shell $v \approx 10^7$ cm/s (100 km/s), and a distance travelled by the envelope during the activity of the maser globule (six months) $l \approx 1.5 \times 10^{14}$ cm (11 AU), which exceeds the size of the maser formations by more than an order of magnitude. For the maser to be in the activated state, the ejected envelope must extend to 11 AU.

The energy release required for observations of the maser line can be estimated as follows. The flux from the source at the Earth is $F_{\rm E} \approx 8 \times 10^4$ Jy. Since we know the distance to W49N ($\sim$11 kpc) and the maser line emission bandwidth ($\sim$50 kHz), we obtain the line luminosity $L_{\rm maser} \approx 0.1\ L_{\odot}$. The ratio of line luminosity and the luminosity of the central star

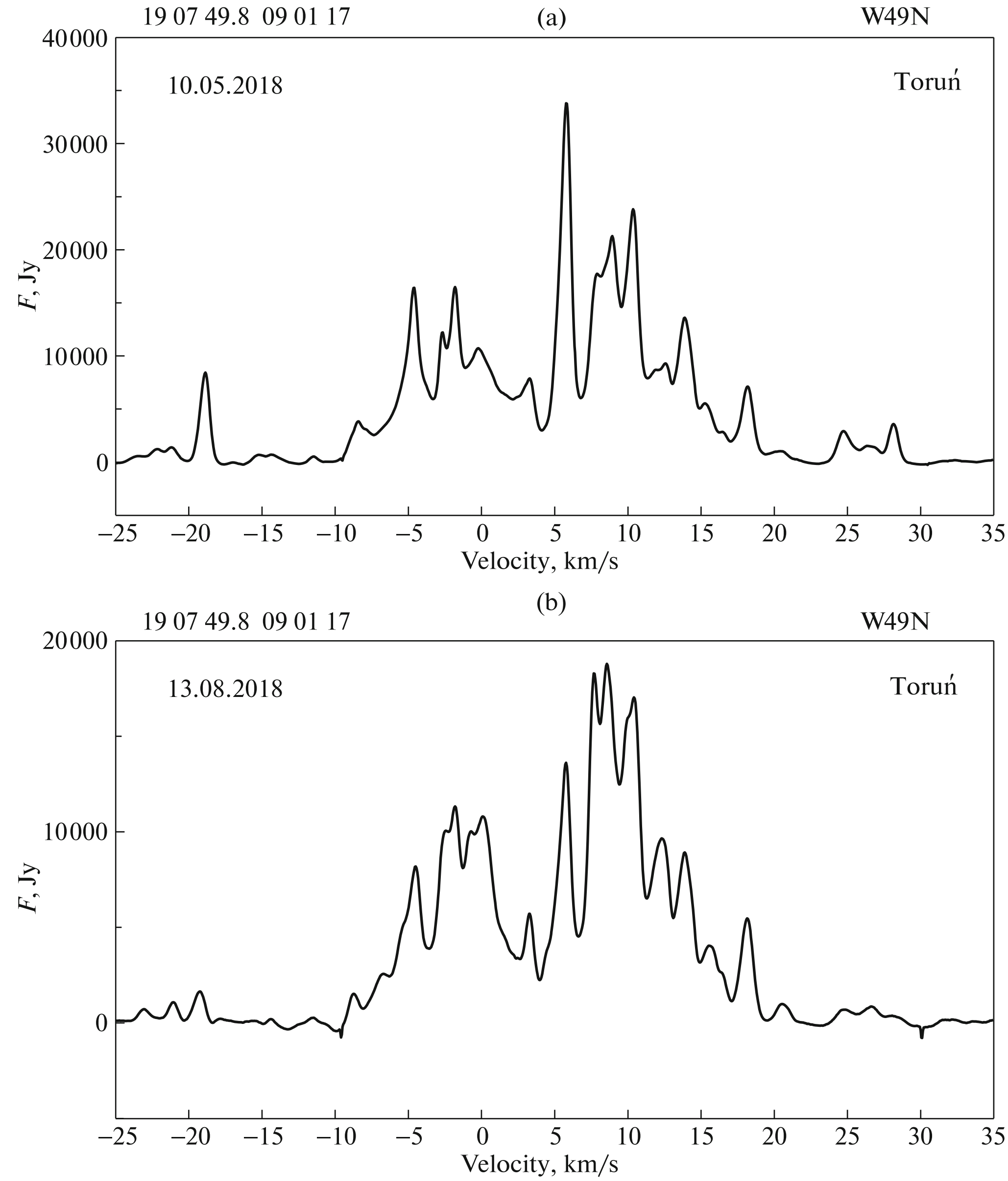

Fig. 13. Spectrum of low-velocity lines in W49N on the descending branch of the water-maser flare on (a) May 10, 2018 and (b) August 13, 2018.

($L_* \approx 10^6\ L_\odot$) is $N \approx 10^{-6}$. We must also consider scattering of the energy propagating from the star to the maser globule. The globule receives a fraction of the energy $(R_{\rm gl}/R)^2 \approx (1.3 \times 10^{13}/1.3 \times 10^{16})^2 \approx 10^{-6}$, where $R_{\rm gl}$ is the size of the globule and R the distance from the central star to the globule. This means that the central star can provide the energy required for the isotropic luminosity of the maser globule. The energy required to excite the globule is $E \approx L_* t \approx 6 \times 10^{46}$ erg, where L_* is the luminosity of the central star and t the duration of the flare.

For example, during its evolution, a massive star emits an energy $E_* \approx 10^{-2} M_* c^2 \approx 0.6 \times 10^{54}$ erg into the surrounding space; i.e., eight orders of magnitude more energy than the amount indicated above. Over the evolution of the central massive star (about a million years), multiple envelope ejections could occur, since the mass of envelope lost is $M_{\rm env} \approx E/v^2 \approx 10^{31}$ g, about 10^{-4} of the mass of the central star.

Knowing the characteristic time between flares, it is possible to approximately estimate the parameters of the orbit of the companion about the central star in W49N. During long-term observations of the source since its discovery, individual powerful flares of its water-maser emission have been recorded. Adopting ten years as the characteristic time between these flares, based on celestial mechanics, we infer a semi-major axis for the elliptical orbit $\sim$30 AU for a massive central star of 50 $M_\odot$ paired with a lower-mass, but still massive, companion. Thus, spending several years close to the pericenter of the system, the companion's gravitational interaction with the central star could initiate a loss of some fraction of the stellar atmosphere into the surrounding medium. Moving at a velocity of hundreds of km/s, this lost mass acts more powerfully than any stellar wind. The asymmetry of the lost envelope material creates an observable asymmetry of the resulting line emission over a wide range, taking into account that the ejections in W49N occur at an angle of 35° to the line of sight [33]. Bearing in mind that companion stars may spend several years near the pericenter, this mechanism for the activation of maser emission cannot be ruled out.

Observational data supporting this picture can be found. In W49N, we observe a maser-line spectrum extending over a wide range of velocities (500 km/s). In our opinion, the most acceptable explanation of this is the mechanism proposed in [31, 32, 34]. According to these studies, high-velocity and low-velocity maser features correspond to the same set of velocities, but the low-velocity features are moving closer to perpendicular to the line of sight due to projection effects. This is also consistent with a picture with an elongated envelope around a massive central star moving preferentially at some angle relative to the line of sight. This angle has been measured for W49N, and is equal to 35° [33]. The low- and high-velocity features expand from a common center [34], possibly testifying a common origin. We can also imagine the following continuation of events. For distances from the central star up to 0.1 pc, the velocities of the maser features is within 20 km/s. Later, they can increase to 200 km/s or more [33, 34]. This acceleration could be due to the propagation of a shock into a less dense surrounding medium [33]. If the hypothesis of acceleration of the maser clouds by shocks due to the motion of the matter ejected by the central star is correct, the estimated thickness of the ejected envelope must be reduced. Interferometric observations also show that both low- and high-velocity features show high proper motions [31, 34]. This may testify to the physical identity of the maser formations (features).

Thus, the mechanism for the primary energy release we have proposed is consistent with the above physical picture for the origin of giant flares in maser features in W49N, Orion KL, G25.65+1.05. Testing of this hypothesis will require further monitoring with single antennas and VLBI studies in a dynamic regime.

6. CONCLUSIONS

(1) We have carried out long-term monitoring of the Galactic kilomaser W49N in the water line corresponding to the $6_{16}-5_{23}$ transition at $f =$ 22.235 GHz using the 22-m Simeiz, 32-m Toruń, 100-m Effelsberg, and 32-m Medicina radio telescopes.

(2) We have determined the detailed shape of the line flux density variations during a unique giant flare from September 2017 through almost all of 2018.

(3) We find evidence that the kilomaser operated in an unsaturated regime during the flare: a characteristic dependence of the line width on the flux was observed.

(4) The coincidence of the line flux variations in the giant flares of two different sources—W49N and Orion KL—was noted, possibly suggesting that similar processes occurred during the flares of these two different water-maser sources.

(5) The shape of the line indicates that the flare occurred in a single source.

(6) We have considered one possible driver of the primary energy release in the system that could lead to the flare of the kilomaser and the substantial increase in its flux. This explosive process in the central massive star could be associated with an ongoing partial loss of its envelope.

FUNDING

This work was supported by the Polish National Science Center (grant 2016/21/B/ST9/01455) and partially supported by Program 12 of the Presidium of the Russian Academy of Sciences and the Russian Foundation for Basic Research (grant 19-52-4014). The study is partially based on observations with the 100-m telescope of the Max Planck Institute for Radio Astronomy.

REFERENCES

1. S. H. Knowles, C. H. Mayer, A. C. Cheung, D. M. Rank, and C. H. Townes, Science **163**, 1055 (1969).
2. A. C. Cheung, D. M. Rank, C. H. Townes, D. D. Thornton, and W. J. Welch, Nature **221**, 626 (1969).
3. F. Sato, F. Akabane, and F. J. Kerr, Austral. J. Phys. **20**, 197 (1967).
4. C. G. Wynn-Williams, Mon. Not. R. Astron. Soc. **151**, 397 (1971).
5. B. Zhang, M. J. Reid, K. M. Menten, et al., Astrophys. J. **775**, 79 (2013).
6. V. S. Strel'nitskii and R. A. Syunyaev, Sov. Astron. **16**, 579 (1972).
7. R. B. Larson, Ann. Rev. Astron. Astrophys. **11**, 219 (1973).

8. J. Silk and J. R. Burke, Astrophys. J. **190**, 11 (1974).
9. W. T. Sullivan, Astrophys. J. Suppl. **25**, 393 (1973).
10. J. M. Moran, G. D. Papadopoulos, B. F. Burke, K. J. Lo, et al., Astrophys. J. **185**, 535 (1973).
11. S. N. Knowles, K. J. Johnston, J. M. Morgan, B. F. Burke, K. Y. Lo, and P. R. and G. D. Papadopoulos, Astron. J. **79**, 925 (1974).
12. S. H. Knowles, C. H. Mayer, W. T. Sullivan, and A. C. Cheung, Science **166**, 221 (1969).
13. R. H. Gammon, Astron. Astrophys. **50**, 71 (1976).
14. M. Harwit, D. A. Neufeld, G. J. Melnik, and M. J. Kaufman, Astrophys. J. **497**, 105 (1998).
15. C. Ceccarelli, E. Caux, G. J. White, S. Molinari, et al., Astron. Astrophys. **331**, 372 (1998).
16. B. Nisini, M. Benedettini, T. Giannini, E. Caux, et al., Astron. Astrophys. **350**, 529 (1999).
17. W. D. Gwinn, B. E. Turner, W. M. Goss, and G. L. Blackman, Astrophys. J. **179**, 789 (1973).
18. N. S. Nesterov, A. E. Vol'vach, I. D. Strepka, V. M. Shul'ga, V. I. Lebed', and A. M. Pilipenko, Radiofiz. Radioastron. **5**, 320 (2000).
19. A. E. Vol'vach, L. N. Vol'vach, I. D. Strepka, A. V. Antyufeev, V. V. Myshenko, S. Yu. Zubrin, and V. M. Shul'ga, Izv. KrAO **104** (6), 72 (2009).
20. A. Kraus, T. P. Krichbaum, R. Wegner, A. Witzel, et al., Astron. Astrophys. **401**, 161 (2003).
21. T. M. Heckman and W. T. Sullivan, Astrophys. Lett. **17**, 105 (1976).
22. P. Goldreich, D. A. Keeley, and J. J. Kwan, Astrophys. J. **179**, 111 (1973).
23. T. Omodaka, T. Maeda, M. Miyoshi, A. Okudaira, et al., Publ. Astron. Soc. Jpn. **51**, 333 (1999).
24. T. Shimoikura, H. Kobayashi, T. Omodaka, P. J. Diamond, L. I. Matveyenko, and K. Fujisawa, Astrophys. J. **634**, 459 (2005).
25. J. M. Bologna, K. J. Johnston, S. H. Knowles, S. A. Mango, and R. M. Sloanaker, Astrophys. J. **199**, 86 (1975).
26. R. C. Walker, K. J. Johnston, B. F. Burke, and J. H. Spencer, Astrophys. J. **211**, l135 (1977).
27. R. Gensel, D. Downes, J. M. Morgan, K. J. Johnston, et al., Astron. Astrophys. **66**, 13 (1978).
28. S. Yu. Parfenov and A. M. Sobolev, Mon. Not. R. Astron. Soc. **444**, 620 (2014).
29. K. Inayoshi, K. Sugiyama, and T. Hosokawa, Astrophys. J. **773**, 70 (2013).
30. L. N. Volvach, A. E. Volvach, M. G. Larionov, G. C. MacLeod, et al., Astron. Rep. **63**, 49 (2019).
31. R. Genzel, D. Downes, M. H. Schneps, M. J. Reid, et al., Astrophys. J. **247**, 1039 (1981).
32. M. Elitzur, D. J. Hollenbach, and C. F. McKee, Astrophys. J. **346**, 983 (1989).
33. C. R. Gwinn, Astrophys. J. **393**, 149 (1992).
34. C. R. Gwinn, Astrophys. J. **429**, 241 (1994).

Translated by L. Yungelson